Biogeosciences Discuss., 11, 7685–7719, 2014
www.biogeosciences-discuss.net/11/7685/2014/
doi:10.5194/bgd-11-7685-2014

Biogeosciences Discussions
Open Access

Land surface phenological response to decadal climate variability across Australia using satellite remote sensing

M. Broich[1,*], A. Huete[1], M. G. Tulbure[2], X. Ma[1], Q. Xin[3], M. Paget[4], N. Restrepo-Coupe[1], K. Davies[1], R. Devadas[1], and A. Held[4]

[1]Plant Functional Biology and Climate Change Cluster, University of Technology, Sydney, P.O. Box 123, Broadway, NSW 2007, Australia
[2]Centre of Ecosystem Science, School of Biological, Earth and Environmental Sciences, University of New South Wales, Kensington NSW 2052, Australia
[3]Ministry of Education Key Laboratory for Earth System Modeling, Center for Earth System Science, Tsinghua University, Beijing 100084, China
[4]CSIRO Marine and Atmospheric Research, Pye Laboratory, Acton, ACT, 2600, Australia
[*]now at: Centre of Ecosystem Science, School of Biological, Earth and Environmental Sciences, University of New South Wales, Kensington NSW 2052, Australia

Received: 31 March 2014 – Accepted: 13 May 2014 – Published: 28 May 2014

Correspondence to: M. Broich (mark.broich@unsw.edu)

Published by Copernicus Publications on behalf of the European Geosciences Union.

Abstract

Land surface phenological cycles of vegetation greening and browning are influenced by variability in climatic forcing. Quantitative information on phenological cycles and their variability is important for agricultural applications, wildfire fuel accumulation, land management, land surface modeling, and climate change studies. Most phenology studies have focused on temperature-driven Northern Hemisphere systems, where phenology shows annually reoccurring patterns. Yet, precipitation-driven non-annual phenology of arid and semi-arid systems (i.e. drylands) received much less attention, despite the fact that they cover more than 30 % of the global land surface. Here we focused on Australia, the driest inhabited continent with one of the most variable rainfall climates in the world and vast areas of dryland systems. Detailed and internally consistent studies investigating phenological cycles and their response to climate variability across the entire continent designed specifically for Australian dryland conditions are missing. To fill this knowledge gap and to advance phenological research, we used existing methods more effectively to study geographic and climate-driven variability in phenology over Australia. We linked derived phenological metrics with rainfall and the Southern Oscillation Index (SOI). We based our analysis on Enhanced Vegetation Index (EVI) data from the MODerate Resolution Imaging Spectroradiometer (MODIS) from 2000 to 2013, which included extreme drought and wet years. We conducted a continent-wide investigation of the link between phenology and climate variability and a more detailed investigation over the Murray–Darling Basin (MDB), the primary agricultural area and largest river catchment of Australia.

Results showed high inter- and intra-annual variability in phenological cycles. Phenological cycle peaks occurred not only during the austral summer but at any time of the year, and their timing varied by more than a month in the interior of the continent. The phenological cycle peak magnitude and integrated greenness were most significantly correlated with monthly SOI within the preceding 12 months. Correlation patterns occurred primarily over north-eastern Australia and within the MDB predominantly over

BGD
11, 7685–7719, 2014

natural land cover and particularly in floodplain and wetland areas. Integrated greenness of the phenological cycles (surrogate of productivity) showed positive anomalies of more than two standard deviations over most of eastern Australia in 2009–2010, which coincided with the transition between the El Niño induced decadal droughts to flooding caused by La Niña. The quantified spatial-temporal variability in phenology across Australia in response to climate variability presented here provides important information for land management and climate change studies and applications.

1 Introduction

Vegetation phenological cycles are periodically reoccurring events. In temperature-limited systems, cycles occur on an annual basis, starting in spring and ending in autumn. Existing algorithms aiming to characterize phenological cycles from remotely sensed spectral vegetation "greenness" indices perform well for ecosystems in temperature-driven mid and high latitudes (Eklundh and Jönsson, 2010; Ganguly et al., 2010). Yet, in ecosystems where rainfall is limited and highly variable such as semi-arid and arid systems (i.e. drylands; United Nations, 2011), phenological cycles may be irregular in their length, timing, amplitude and reoccurrence interval, occur at any time of the year or not occur at all in a given year (Brown and de Beurs, 2008; Ma et al., 2013; Walker et al., 2014; Bradley and Mustard, 2007). Despite the fact that drylands cover over 30 % of the global land surface and occur on every continent, their rainfall-driven phenology that features non-annual cycles has been poorly characterized. Here we focused on Australia, a continent where drylands cover more than 80 % of the land surface. We used existing methods more effectively to quantify the phenology of Australia, as an example of a rainfall-driven dryland system. Moreover, recent reports by the Intergovernmental Panel on Climate Change highlighted not only the importance of quantifying vegetation phenology in general (IPCC, 2007, 2013; Schwartz, 2013) but pointed to a lack of phenological studies for Australia and New Zealand (Keatley et al., 2013; IPCC, 2001, 2007).

BGD
11, 7685–7719, 2014

Vegetation phenology refers to the response of vegetation to inter- and intra-annual variation of the Earth's climate, including irradiance, temperature and water (Myneni et al., 1997; White et al., 1997; Zhang et al., 2003). Vegetation phenology is a useful indicator in the study of the response of ecosystems to climate change (Zhang et al., 2012; Richardson et al., 2013), and an important parameter for land surface, climate and biogeochemical models that quantify the exchange of water, energy and gases between vegetation and the atmosphere (Pitman, 2003; Eklundh and Jönsson, 2010). Other applications that require the characterization of vegetation phenology include crop yield quantification, wildfire fuel accumulation, vegetation condition, ecosystem response to climate variability and climate change and ecosystem resilience (Schwartz, 2003; Liang and Schwartz, 2009; Peñuelas et al., 2009).

Phenology at the landscape to continental scale (land surface phenology, hereafter *phenology*) is typically derived using time-series of remotely sensed vegetation greenness indices such as the normalized difference vegetation index (NDVI) and the enhanced vegetation index, EVI (de Beurs and Henebry, 2008). Several studies have used NDVI time series recorded by the Advanced Very High Resolution Radiometer (AVHRR) (Moulin et al., 1997; Zhang et al., 2012), but due to better geometric correction and increased resolution, more recent studies used EVI time series recorded by the MODerate-resolution Imaging Spectroradiometer, MODIS (Tan et al., 2011; Friedl, 2012). Compared with NDVI, EVI is less sensitive to residual atmospheric contamination and soil background variations, and has a larger dynamic range of sensitivity to vegetation greenness (Huete et al., 2002). EVI trajectories measure change in an integrated property commonly referred to as "greenness" that has been found to be correlated with sub pixel leaf chlorophyll content and leaf area index (Huete et al., 2014).

Once derived, phenological cycle parameters (metrics) can be used to quantify the influence of climate variability on phenology (Ma et al., 2013; Brown et al., 2010). Australia has one of the most variable climates in the world, subject to high inter-annual rainfall variability due to the influence of El Niño Southern Oscillation (ENSO) (Nicholls,

BGD
11, 7685–7719, 2014

1991; Nicholls et al., 1997). Previous studies investigated the relationship between vegetation index time series and rainfall globally, and the correlation with soil moisture for Australia (Andela et al., 2013; Chen et al., 2014). However, studies quantifying the relationship between phenology and ENSO-related climate variability as shown for example for Africa (Brown et al., 2010; Philippon et al., 2014) are missing. Here we analyzed a period of time from 2000 to 2013, which encompassed the Australian Millennium Drought from 2001–2009 and the 2010–2011 La Niña flood events (Heberger, 2011; Australian Bureau of Meteorology, 2014a) and focused on one of the most affected areas, the MDB in south-east of Australia (van Dijk et al., 2013; Australian Bureau of Meteorology, 2014a; Kirby et al., 2012). Besides being the catchment of Australia's largest river system and associated ecologically valuable floodplain and wetland ecosystems, the MDB contains the main agricultural area of the continent (Connell, 2007).

The objectives of this study were to: (1) characterize the inter- and intra-annual variability of phenological cycles of greening and browning, including non-annual cycles across all of Australia, a continent with vast areas of dryland ecosystems; and (2) investigate the relationships between the derived phenological metrics and remotely sensed rainfall, as well as between phenological metrics and the Southern Oscillation Index (SOI; Trenberth and Caron, 2000), an atmospheric circulation index and proxy of ENSO, across the entire continent and in more detail for the MDB.

2 Methods

2.1 Study area and data used

Australia covers an area of > 7.6 million km^2 and climatic zones range from tropical in the north to temperate in the south. Average rainfall does not exceed 600 and 300 mm per year across 80 % and 50 % of the land, respectively (Australian Bureau of Meteorology, 2014b). Northern Australia is dominated by savanna, whereas most of the country is covered by grassland and desert vegetation (Köppen, 1884). Forest occurs

BGD
11, 7685–7719, 2014

at higher elevation in the temperate south-west and south-east where large areas of the lowlands are used for rain-fed agriculture (Fig. 1, Lymburner et al., 2011). The MDB contains Australia's primary agricultural area and occupies 14 % of Australia in the south-east of the continent (Fig. 1).

For algorithm development and calibration, we used a set of trajectories at 36 sites distributed across Australia (Fig. 1). These 36 sites represented a range of land cover and climatic zones to ensure that the algorithm captures the variability in phenology across the country. The majority (21) of our test sites were flux tower sites from the OzFlux network (2014). We selected 15 additional test sites to represent a wider coverage of climate conditions, vegetation cover and land uses not represented by the Australian eddy covariance network.

As input data for the phenological characterization we sourced EVI MOD13C2 and MOD13A1 with a temporal resolution of 16 days for the 18 February 2000–22 April 2013 time period (NASA Land Processes Distributed Active Archive Center, 2014). We used the 5.6 km product (MOD13C2) to characterize the biogeographic patterns of vegetation phenology across the entire Australian continent and the 500 m product (MOD13A1) to investigate the phenological patterns in more detail across the MDB.

To analyze the responses of phenological metrics to rainfall variability, we used monthly data from the Tropical Rainfall Measuring Mission Project (TRMM_3B43.v7 product; Goddard Space Flight Center, 2014) for 1999–2012. Instead of using gridded rainfall data interpolated from widely spaced weather stations across large areas of the interior, we opted for remotely sensed rainfall measured by TRMM, which is systematic across space and time.

To analyze the responses of phenological metrics to ENSO, we used monthly data of the Southern Oscillation Index (SOI) obtained from the Australian Bureau of Meteorology (2014c). SOI represents the standardized difference of air pressures between Darwin and Tahiti and serves as a proxy of convection in the western Pacific caused by ENSO sea surface temperature anomalies (Trenberth and Caron, 2000).

BGD
11, 7685–7719, 2014

Across the MDB we used the Dynamic Land Cover dataset provided by Geoscience Australia (Lymburner et al., 2011) to investigate the differences between the phenological responses to SOI and rainfall over natural and managed land cover types. We derived the natural land cover class by grouping land cover dominated by trees, shrubs and grasses. The managed land cover class encompassed rain-fed and irrigated agriculture and pasture. Almost a third of the basin's area is managed for cropping and pasture (Lymburner et al., 2011). We also analyzed the phenological response over the ecologically valuable floodplain and wetland areas of the MDB (Kingsford et al., 2004) and evaluated the floodplain's response to SOI as a proxy of ENSO-related drought and flooding.

2.2 Phenology metrics and algorithm

2.2.1 Phenology metrics

To account for non-annual vegetation dynamics, we defined a phenology cycle not as an annually or seasonally reoccurring event but more broadly as a cycle of EVI-measured greening and browning that may occur more than once per year or may skip a year entirely and not occur for one or more years.

We modeled phenological cycle curves and key properties of each phenological cycle in the form of curve metrics. The phenological metrics modeled the timing and magnitude of key transitional points on the cycle's curve and included the timing and magnitude of the minimum points before and after a phenological cycle, the peak point of the cycle and the start and end point of the cycle. In addition, we also calculated the integrated area between the start and end points of a cycle as a surrogate of vegetation productivity during a cycle (Zhang et al., 2013). By tracking the phenological cycle metrics over time, we characterized the intra- and inter-annual variability of the phenological cycle and thereby vegetation growth patterns.

BGD
11, 7685–7719, 2014

2.2.2 Data pre-processing

We used the MOD13 products' QA flags to discard observations with insufficient quality, which included any observation with either VI usefulness > code "10", snow cover, high aerosol or climatology aerosol quantity, mixed or high clouds present or water in the Land/Water Flag. For each pixel, we first gap-filled the data points discarded in the previous step. We used cubic spline interpolation as the temporal gap filling method (Dougherty et al., 1989). Next, we smoothed the time series for each pixel using Savitzky–Golay smoothing filter (Savitzky and Golay, 1964). This step reduced the noise in the trajectories that would otherwise impact the identification of minimum and maximum points and the subsequent fitting of a mathematical curve to characterize the phenological cycles.

2.2.3 Curve fitting and phenological metric derivation

We identified minimum and maximum points of the per-pixel time series using a moving window and a > 0.01 EVI amplitude threshold to identify cycles of greening and browning. We used the identified minimum points to define the temporal extent of phenological cycles and then fitted the mathematical function within this interval. Thereby, we did not expect a phenological cycle in a fixed interval of the year but allowed the cycle to occur and be characterized without a predefined interval to better represent the highly variable rainfall-driven phenological patterns across Australia's vast drylands. We fitted 7 parameter double logistic curves to each cycle in the per-pixel time series, defined as:

$$\mathrm{EVI}(t) = V_{\mathrm{min_a}} - \frac{V_{\max} - V_{\mathrm{min_a}}}{1 + \exp\left(\frac{T_{\mathrm{mid_a}} - t}{S_{\mathrm{a}}}\right)} + \frac{V_{\max} - V_{\mathrm{min_b}}}{1 + \exp\left(\frac{T_{\mathrm{mid_b}} - t}{S_{\mathrm{b}}}\right)} \quad (1)$$

where $V_{\mathrm{min_a}}$ and $V_{\mathrm{min_b}}$ are equal to the first and second minimum EVI, respectively. Vmax is the high asymptote in the double logistic model, $T_{\mathrm{mid_a}}$ is the time when EVI

BGD
11, 7685–7719, 2014

reached half of $V_{max} - V_{min_a}$. T_{mid_b} is the time when EVI reached half of $V_{max} - V_{min_b}$. S_a and S_b are the scale parameters on the increasing and the decreasing side of the curve, respectively. If a second phenological cycle was identified within a year, a second 7 parameter double logistic curve was fitted to characterize this cycle. We identified the start and end points of each cycle as the points where the EVI reached 20 % of the amplitude, between the first minimum and the peak, and the peak and the second minimum, respectively.

An example of the algorithm processing steps is shown for the Alice Springs flux tower site (Fig. 2). The site represents *Acacia* woodlands in the arid interior of Australia. The site serves as an example for how our algorithm characterized the high temporal variability in phenological cycles for the interior of Australia.

2.3 Analysis of spatial-temporal patterns of phenology across Australia

After deriving phenological cycles and their metrics from per-pixel greenness trajectories we analyzed the metrics across Australia at two levels of temporal aggregation: (1) in the form of summary statistics (mean and standard deviation) across greenness trajectory to quantify overall phenological variability over the 14 year time series; and (2) in the form of inter-cyclic variability as the difference between a metric of one cycle and the following cycle over the 14 year time series.

For a given site we calculated for example the mean peak magnitude and the peak magnitude's standard deviation. An example of inter-cycle variability of metrics is our analysis of peak timing for all peaks across the time series. We also analyzed the deviation of an individual phenological cycle integral relative to the expected variability. For this purpose, we calculated the standardized anomaly of each cycle's integral as the difference of the cycle's integral from the mean integral divided by the standard deviation of the integrals.

BGD
11, 7685–7719, 2014

2.4 Analysis of spatial-temporal patterns of Australian phenology in response to rainfall and SOI variability

We further analyzed the statistical relationship between phenological cycle peak magnitude and cycle integrated greenness and TRMM rainfall and SOI (four combinations of correlation analyses) across Australia and in more detail for the MDB. The cycle peak magnitude represents maximum greenness while the cycle integrated greenness serves as a proxy of ecosystem productivity (Zhang et al., 2013). We used non-parametric Spearman ranked correlation tests (Lehmann and D'Abrera, 1975), hereafter Spearman ρ, to determine the strength of significant monotonic relationships between rainfall and each of the two phenology metrics as well as SOI and the two phenology metrics. We evaluated relationships between rainfall and SOI as the explanatory variables binned over different intervals and with different lead times to the phenological cycle integral and peak magnitude, which were used as the response variables. We binned rainfall accumulation for intervals of 1 to 12 months and average SOI values for periods of 1 to 12 months up two 12 months prior to the phenological cycle peak.

The underlying assumption for investigating Spearman ρ correlations between phenology and rainfall or SOI was that a significant and strong monotonic relationship between a phenological metric and preceding rainfall or SOI suggested that the phenology metric (peak magnitude and integrated greenness) is likely driven by the respective climate variable.

Aiming to identify correlation patterns and how these patterns change as a function of binning interval (1–12 months) and lead times (up to 12 months), we extracted for each pixel and binning interval the most significant test result. For each potential driver and binning interval, we analyzed the lead time, correlation and significance value. We visualized the results only for areas that were significant (p value < 0.05) and had a rho value of > 0.6.

Using the above methodology, we conducted a continent-wide analysis and a higher resolution analysis investigating the relationship of SOI with phenology metrics for the

BGD
11, 7685–7719, 2014

MDB in south-eastern Australia. Within the MDB we further investigated relationship between SOI and phenology (differences in correlation patterns) over natural and managed land cover types as well as the catchment's floodplain and wetlands.

3 Results

3.1 Mean and variability of peak magnitude and minimum magnitude across 14 years

We evaluated the mean and variability of the peak and minimum magnitude across the 14 year time series to investigate the inter-annual variations in vegetation phenology. The highest mean peak magnitude occurred in a narrow area covered predominantly by evergreen humid tropical forest along the north-eastern coast (light color areas in Fig. 3a). The same area also had the highest mean minimum magnitude values, indicating that greenness was persistently high (light color areas in Fig. 3b). Other areas with high levels of persistent greenness included temperate grasslands in coastal locations of south-east Australia, temperate broadleaf forest in the south-east and south-west of the continent, and across most of Tasmania (light color areas in Fig. 3a and b). The largest mean amplitude (peak minus minimum magnitude) occurred in areas used for crop cultivation and grazing in the south-west and the south-east. Areas of low mean peak amplitude were found across large parts of the interior (darker tone areas in both Fig. 3a and b) with the exception of the desert river beds.

The highest level of variability in peak magnitude occurred over cropped areas in the south-east and south-west of Australia (light colored areas in Fig. 3c). High variability of peak magnitude over natural vegetation cover was observed for regions predominantly covered with tropical tussock grasses in the inland north and north-east as well as areas with predominant chenopod woody shrubs cover along the Great Australian Bight along the southern coast of Australia (light color areas in Fig. 3c). High variability in minimum magnitude occurred at higher elevations of the southern Great Dividing

BGD
11, 7685–7719, 2014

Range in south-east of Australia (light color areas in Fig. 3d) and around the center of the arid Lake Eyre, which is the lowest point of the continent.

3.2 Inter-cycle variability in peak timing

The timing of the cycles' peak showed large variation from one year to another across most of Australia (Fig. 4). Variations in peak timing were observed over most of interior Australia. Later than average peak timing occurred in 2001, 2004 and 2005 (Fig. 4). Earlier than average peak timing was observed in 2010–2012 over interior Australia (Fig. 4). The peak timing in the wet tropical savannas of the Northern Territory and for most of the south-west wheat belt was relatively stable (Fig. 4). The center of the continent showed an earlier than average peak in 2002 and 2009.

Over interior Australia peak timing varied by over a month from one year to another. Areas for which no peak was observed in a given year (shown in gray in Fig. 4) occurred primarily in the drylands of the continent's interior, where phenological cycles may not follow an annually reoccurring pattern. For example, areas with no peak over interior Australia in Fig. 4 for 2005 and 2008 can be also traced in Fig. 2 where the phenological trajectory of the Alice Springs site did not show a peak in those years.

3.3 Variability of cycle-integrated greenness

Greenness integrated between the start and end of a phenological cycle can provide a first approximation of vegetation productivity (Ponce Campos et al., 2013; Zhang et al., 2013). Standardized anomalies of integrated greenness highlight the deviation of an individual value from the mean, relative to the expected level of variability (the standard deviation). Standardized anomalies of integrated greenness were highly variable across time (Fig. 5). Negative standardized anomalies of integrated greenness (red tones in Fig. 5) occurred across the continent in most areas in 2002 and vast areas of the continent in 2008 and 2009. Large areas of negative anomalies also occurred in 2001 to 2003 and from 2004 to 2009. Large areas of positive standardized anomalies

BGD
11, 7685–7719, 2014

(green tones in Fig. 5), with increased greening of 1 to 2 standard deviations, occurred in 2010 a year of particularly high rainfall.

When relating the cycles' standardized anomalies of integrated greenness to the phenological trajectory at the Alice Springs tower site, the widespread negative standardized anomaly over interior Australia in 2008 (Fig. 5) was not represented in the site's curve (Fig. 2) where no cycle started or ended in 2008 and 2009. Conversely, the positive standardized anomalies of cycles that started in 2010 and 2011 over large areas of eastern and interior Australia can also be seen in the Alice Springs curve in the form of larger than average integrals (Fig. 2).

3.4 Analysis of spatial-temporal patterns of Australian phenology relative to rainfall and SOI variability

We conducted correlation analysis relating two climate drivers (SOI and rainfall) and two phenological metrics (peak magnitude and cycle integral), respectively (four combinations). Each of the four analysis included climate drivers binned over periods between 1 and 12 months within the 12 month period leading up to the phenological peak. We found that areas with significant correlations between SOI and phenology or rainfall and phenology were most widespread for a binning interval of one month. Areas with significant correlations shrank as we increased the binning interval of SOI or rainfall from 1 to 12 months.

The spatial pattern of significant correlations (areas significantly correlated, correlation strength, and lead times) was generally similar for all four combinations of variables. However, the patterns of significant correlation between peak magnitude and climate variables covered a larger area compared to patterns of significant correlation between cycle integral and climate variables. The patterns of significant SOI-driven correlation with phenology covered a larger area compared to the rainfall driven correlation patterns. Given the above similarities and the largest extent of significant correlation patterns at a single month binning interval, we limit the presentation of results to the most significant monthly SOI–cycle peak magnitude correlation.

BGD
11, 7685–7719, 2014

The most significant correlation of monthly SOI and cycle peak magnitude were most widespread in north-eastern Australia (Fig. 6c). Lead times between the most significantly correlated SOI month and the phenological cycle peak were 1 to 6 months for north-eastern Australia and 7 to 12 months for the East Australian interior representing an increase in lead time along a gradient of decreasing rainfall (Fig. 6a and b). These correlation patterns extended into the Australian interior along desert river drainage lines such as the Cooper Creek. Cooper Creek's floodplain can be clearly distinguished in the correlation pattern, indicating a strong response of the floodplain vegetation to SOI variability (Fig. 7). Additional correlation patterns with a shorter lag time (1–3 months) were observed near the west coast of Australia (Fig. 6a).

In the MDB, correlation patterns between monthly SOI and cycle peak magnitude occurred primarily over natural vegetation cover as opposed to areas used for agriculture or pasture (managed land cover). The percentage of all significant relationships over natural land cover was 83.6 % as opposed to 15.9 %, the percentage of all significant relationships over managed land cover (Table 1). These percentages were disproportional to areal percentages of natural and managed land cover within the MDB (71.8 % and 28.2 %, respectively). The highest percentage of significantly correlated areas within each land cover class and highest mean rho values were found in areas dominated by shrubs, trees and grasses. Irrigated agriculture and pasture had the smallest percentage of correlated area (Table 1) compared to other land cover classes.

The ecologically valuable floodplains and wetlands of the MDB made up 10.9 % of the basin area and were of mixed land cover composition. The percentage of all areas with significant correlations between monthly SOI and phenological cycle peak magnitude in floodplains and wetlands was disproportionally higher (14.8 %) than the percentage of area occupied by this zone (10.9 %). In addition, 6.1 % of the floodplain and wetlands area showed significant relationships with monthly SOI, which is higher than for any of the individual land cover classes in Table 1.

BGD
11, 7685–7719, 2014

4 Discussion

4.1 A phenological characterization of Australia that accommodates non-annual phenological cycles

Our research characterized the cycles and variability of non-annual vegetation phenology across Australia and identified relationships with variability in rainfall and ENSO-related large scale atmospheric circulation. We provide a characterization of annual and non-annual phenological cycles of vegetation greening and browning for Australia based on MODIS EVI data.

We used an enhanced phenology model to characterize rainfall-driven phenology across the Australian continent, which includes large dryland regions. Very few studies have previously quantified the land surface phenology of dryland systems (Walker et al., 2014), likely due to the fact that the phenology of these systems is more complex than that of most temperature-limited regions (Primack and Miller-Rushing, 2011; Walker et al., 2014). Dryland phenology responds to a variable rainfall regime where the timing and magnitude of precipitation events varies inter-annually (Loik et al., 2004; Brown et al., 1997).

We identified and characterized rainfall-driven phenological cycles at any time of the year over a 14 year time series rather than within a predefined interval of every calendar year. This is important as the timing of phenological cycles varied and not every phenological cycle metric occurred in every year. We first identified points demarking phenological cycles from the entire EVI time series and then characterized the cycles using mathematical curves. For example, we did not identify a cycle peak for every year and every pixel (areas shown in gray in Fig. 4). However, this does not imply that no cycle occurred but that the vegetation at these sites and points in time could be greening up towards a peak in the following year, browning down towards an end of cycle point or be in a phase between cycles. For example, the absence of peaks over interior Australia in 2005 and 2008 (Fig. 4) is also reflected in Fig. 2 where the phenological trajectory of the Alice Springs site in interior Australia was in between phenological

BGD
11, 7685–7719, 2014

cycles. Phenological cycles thus need to be analyzed in the temporal context of multiple years. While most studies of phenology attempted to fit phenological curves within a predefined interval every calendar year, certain authors have proposed methods that include iterating the curve fitted to the vegetation index trajectory or by fitting a curve of vegetation index vs. accumulated moisture (Brown and de Beurs, 2008; Tan et al., 2011). Our approach to characterize non-annual phenology can be applied to other areas with rainfall-driven phenology and thus contributes to our understanding of non-annual, rainfall-driven phenological dynamics globally.

4.2 Phenology of Australia's interior

For the interior of Australia we identified low phenological peak and minimum magnitude and associated small amplitude (darker tone areas in both Fig. 3a and b), high variability in magnitude, timing and cycle integral. In addition, a peak was not identified in every year for large areas of the interior. Most areas of the interior are dryland systems with sparse vegetation cover and where vegetation phenology is driven by highly irregular rainfall timing and amounts (Australian Bureau of Meteorology, 2014d) and hydrologic regimes can be difficult to predict (Young and Kingsford, 2006). Thus we do not see a strong phenological response (low amplitude), however we see a fast response to rainfall pulses and dormant periods during dry years (Loik et al., 2004). We interpret these patterns of variable phenological cycles over interior Australia, where a cycle may vary in timing and length, or may skip a year entirely, to occur as a function of high climate variability. De Jong et al. (2012) identified frequent trend breaks of greening and browning over Australia that may be related to the non-annual phenological cycles identified here.

Desert river beds in the interior of the continent had low minimum but moderate peak magnitude. The elevated peak magnitudes are caused by flooding driven by high amounts of distant rainfall (Young and Kingsford, 2006). The center of the arid Lake Eyre basin showed high variability in minimum magnitude. Lake Eyre is the center of a sparsely vegetated, close drainage basin and the fact that we identified high variability

BGD
11, 7685–7719, 2014

was in line with known flooding patterns as this salt lake is reached by flooding only once in a century (McMahon et al., 2005). We interpret the positive anomaly in 2010 (Fig. 5) as a function of the La Niña floods (Australian Bureau of Meteorology, 2014a).

Conversely, large variability of peak timing and cycle integrated greenness from one to another phenological cycle was found not just in the interior of Australia but across most of the continent (Figs. 4 and 5). High inter-annual variability in water availability across most of Australia rather than for the continent's interior has also been demonstrated by the Australian Water Availability Project (2014).

4.3 Australia's phenology, the 2001 to 2009 Millennium Drought and La Niña high precipitation event in 2010

The years with widespread negative standard anomalies of cycle integrated greenness coincided with the Millennium Drought from 2001 to 2009 (Heberger, 2011, Fig. 5). Dryland vegetation is subject to environmentally marginal conditions and is therefore highly sensitive to climate variability (Brown et al., 1997; Hufkens et al., 2012). Yet, the spatial extent of negative anomalies in certain years that extend beyond the dry interior suggested temporary yet severe drought-related water limitations also in the monsoonal north and the temperate area of south-eastern and south-western Australia (Fig. 5). The large positive standardized anomalies of cycle integrated greenness identified in this work across most of eastern Australia in 2010 (1 to 2 standard anomalies; Fig. 5) coincided with a strong La Niña event and associated high rainfall and floods that broke the Millennium Drought (Australian Bureau of Meteorology, 2014a; Heberger, 2011). This pattern includes the desert rivers extending from north-eastern Australia to Lake Eyre, which experienced a major flood in 2010.

While the relationship between ENSO cycles and rainfall variability primarily over eastern Australia has been investigated before (van Dijk et al., 2013; Risbey et al., 2009), our research has quantified vegetation response across Australia to the transition from a strong El Niño drought to La Niña wet periods. While the positive vegetation response to the 2010 La Niña occurred over eastern Australia that is also influenced by

BGD
11, 7685–7719, 2014

ENSO cycles (van Dijk et al., 2013; Nicholls, 1991; Nicholls et al., 1997), the negative vegetation response during the Millennium Drought cover a larger area and occurred across the continent.

4.4 Spatially explicit relationship between phenology and climatic variability

We found that SOI-driven patterns of correlation with phenology covered a larger area compared to rainfall-driven patterns likely because SOI is a more generic proxy of climatic variability influencing temperature, incoming solar radiation and rainfall rather than rainfall alone (Australian Bureau of Meteorology, 2014e; Risbey et al., 2009) and because not all ecosystems of Australia are only limited by water availability but also by temperature and radiation (Nemani et al., 2003).

The spatial extent of areas where we detected correlation between SOI or rainfall and phenological metrics shrank with longer binning intervals of the climatic drivers. This suggested that relationships between climatic drivers and phenological variability were strongest for driver variability within a specific month of the year (e.g. SOI in September) as opposed to driver variability within for example a 6 month period (e.g. mean SOI across 6 months starting in April). This falls in line with the findings by Stone et al. (1996) who identified relationships between short-term SOI dynamics at specific times of the year and rainfall. Previous studies (e.g. Brown et al., 2010) using seasonal or longer temporal aggregation of driver variables may therefore have not identified the full spatial extent of correlation patterns.

We found the most widespread significant correlation patterns between SOI and peak magnitude in north-eastern Australia, which is in the proximity of the west Pacific convection variability indicated by SOI. The lag times of correlations over north-eastern Australia varied between 1 and 6 months. Shorter lag time (1 to 3 months) correlation patterns were observed near the west coast of Australia. These patterns are spatially remote from the variability in convection over the western Pacific (north-east of Australia) indicated by SOI. They may be related to the interaction between SOI and the Indian Ocean Dipole (Risbey et al., 2009). The identified lag time of predominantly 3

BGD
11, 7685–7719, 2014

to 6 months between SOI and phenological cycle peak magnitude over north-eastern Australia and 7 to 12 months for the East Australian interior falls within the range of aggregation used by Andela et al. (2013) who related NDVI with rainfall. A study by Chen et al. (2014) identified short lags (predominantly 1 month) between soil moisture and NDVI, which are shorter than most of the lags we identified here. Soil moisture in the previous month may provide the most direct relationship with vegetation response (as it represents water available to vegetation) but the climatic conditions that drive soil moisture may precede the soil moisture by a few months (Philippon et al., 2014). The identified increase in lag time between SOI and phenological peak magnitude along a gradient of decreasing rainfall was in agreement with the findings by Andela et al. (2013). However, these findings contradict the concept that rainfall pulse drive rapid phenological response (Loik et al., 2004) or may suggest that vegetation responds to climatic variability at multiple time scales.

The proportion of areas for which we identified significant correlations was generally smaller than those identified in other studies (e.g. Andela et al., 2013; Chen et al., 2014). This could be related to the relatively short time series we used and consequently the smaller power of our correlation analysis. Nonetheless, the spatial pattern of correlation was most widespread in north-eastern Australia and along desert river beds (e.g., Cooper Creek) in the interior. These spatial patterns agreed spatially with what would be expected from the SOI-approximated moisture source over the West Pacific and the associated progression of rainfall and runoff into interior Australia.

We conducted a higher spatial resolution correlation analysis for the MDB to investigate sensitivity of the area's vegetation to SOI variability. The MDB contains the primary agricultural area of Australia and the basin's agriculture was severely impacted by the Millennium Drought (van Dijk et al., 2013; Kirby et al., 2012; Heberger, 2011). We identified correlation patterns between SOI and peak magnitude primarily over natural vegetation cover as opposed to areas used for dryland agriculture or pasture. As expected, irrigated agriculture had the lowest percentage of area with significant correlations between SOI and phenological peak magnitude. The lowest percentage of

BGD
11, 7685–7719, 2014

area with significant correlations over managed land may be explained by the effort that land managers and irrigators make to archive maximum production regardless of climatic variability (e.g. fertilization, use of pesticides, crop rotation, livestock density, movement and irrigation) whereas landscapes with natural vegetation cover may respond directly to climatic variability. In the context of climatic influence on agriculture in the MDB, van Dijk et al. (2013) suggested that the Millennium Drought impact on dryland wheat yields was offset by steady increases in cropped area and plant water use efficiency as well as possibly CO_2 fertilization. As a zone of special interest within the MDB we focused on floodplains and wetlands. These ecosystems were strongly impacted by the Millennium Drought and 2010 La Niña floods (Australian Bureau of Meteorology, 2014a; Leblanc et al., 2012). Across the MDB's floodplains and wetlands, we identified the highest percentage of areas (6.1 %) with significant correlation between SOI and phenological peak magnitude compared to other natural or managed land cover, highlighting the sensitivity of these ecosystems to ENSO-related climatic variability. We attributed the low percentage to limited test power as a function of the relatively short time series (14 years) used here. For example Brown et al. (2010) found between 10 % and 27 % of certain areas in Africa to be significantly correlated with atmospheric indices using a 25 year AVHRR time series.

4.5 Limitations and future work

Several caveats of our work should be noted. When interpreting the phenological cycles characterized here, it should be noted that the sub pixel composition of vegetation and background as well as multi-layer vegetation structure is unknown and may change over time (Zhang et al., 2009; Walker et al., 2012, 2014). Various methods for validating remotely sensed metrics of phenological cycles with ground based observations have been discussed including flux tower productivity time series, ground based radiation sensor time series, phenocam time series as well as crowd sourced citizen science (Richardson et al., 2007; Liang and Schwartz, 2009; Restrepo-Coupe et al., 2014). Validation of the phenological metrics developed here is currently underway.

BGD
11, 7685–7719, 2014

The phenological metrics derived and described here represent different stages of vegetation growth. They have been made freely available in contribution to the Australian Terrestrial Ecosystem Research Network (TERN) and can be downloaded from the AusCover TERN Sydney node[1]: http://data.c3.uts.edu.au providing opportunities for a range of applications.

In this work we traced phenological cycles over time, quantified cycles' inter-annual variability and investigate their relationship with rainfall and ENSO thereby advancing phenological research for Australia, a country with extensive drylands. The phenological metrics provided here can be further used for characterizing the effect of anthropogenic disturbances on phenology and unraveling this effect from the influence of climatic forcing related to ENSO. Another opportunity for future work is the reanalysis of trends and trend breaks in vegetation dynamics and climatic drivers (Donohue et al., 2009; de Jong et al., 2012; Chen et al., 2014).

Acknowledgements. This research was supported by an Australian Research Council Discovery grant (DP1115479) entitled "Integrating remote sensing, landscape flux measurements, and phenology to understand the impacts of climate change on Australian landscapes" (Huete, CI) and funding from the AusCover Facility of the Australian Terrestrial Ecosystem Research Network (TERN). Calculations were performed on the University of Technology, Sydney eResearch high performance computing facility. Tulbure was partially funded through an Australian Research Council Discovery Early Career Researcher Award (DE140101608).

References

Andela, N., Liu, Y. Y., van Dijk, A. I. J. M., de Jeu, R. A. M., and McVicar, T. R.: Global changes in dryland vegetation dynamics (1988–2008) assessed by satellite remote sensing: comparing a new passive microwave vegetation density record with reflective greenness data, Biogeosciences, 10, 6657–6676, doi:10.5194/bg-10-6657-2013, 2013.

[1]The Australian Phenology Product is scheduled to permanently migrate to the Australian *Research Data* Storage *Infrastructure (RDSI)* that is funded through the Australian Government's Super Science Initiative and sourced from the Education Investment Fund (EIF).

BGD
11, 7685–7719, 2014

Australian Bureau of Meteorology: The 2010–11 La Niña: Australia Soaked by One of the Strongest Events on Record, available at: http://www.bom.gov.au/climate/enso/feature/ENSO-feature.shtml, 2014a.
Australian Bureau of Meteorology: Climate of Australia, Australian Government Bureau of Meteorology, available at: http://www.bom.gov.au/lam/climate/levelthree/ausclim/ausclim.htm, 2014b.
Australian Bureau of Meteorology: Southern Oscillation Index Data, available at: http://www.bom.gov.au/climate/current/soi2.shtml, 2014c.
Australian Bureau of Meteorology: Rainfall Variability, available at: http://www.bom.gov.au/jsp/ncc/climate_averages/rainfall-variability/index.jsp, 2014d.
Australian Bureau of Meteorology: ENSO impacts – temperature, available at: http://www.bom.gov.au/climate/enso/history/ln-2010-12/ENSO-temperature.shtml, 2014e.
Australian Water Availability Project, available at: http://www.eoc.csiro.au/awap/, 2014.
Bradley, B. A. and Mustard, J. F.: Comparison of phenology trends by land cover class: a case study in the Great Basin, USA, Glob. Change Biol., 14, 334–346, doi:10.1111/j.1365-2486.2007.01479.x, 2007.
Brown, J. H., Valone, T. J., and Curtin, C. G.: Reorganization of an arid ecosystem in response to recent climate change, P. Natl. Acad. Sci. USA, 94, 9729–9733, 1997.
Brown, M. E. and de Beurs, K. M.: Evaluation of multi-sensor semi-arid crop season parameters based on NDVI and rainfall, Remote Sens. Environ., 112, 2261–2271, doi:10.1016/j.rse.2007.10.008, 2008.
Brown, M. E., de Beurs, K., and Vrieling, A.: The response of African land surface phenology to large scale climate oscillations, Remote Sens. Environ., 114, 2286–2296, doi:10.1016/j.rse.2010.05.005, 2010.
Chen, T., de Jeu, R. A. M., Liu, Y. Y., van der Werf, G. R., and Dolman, A. J.: Using satellite based soil moisture to quantify the water driven variability in NDVI: a case study over mainland Australia, Remote Sens. Environ., 140, 330–338, doi:10.1016/j.rse.2013.08.022, 2014.
Connell, D.: Water Politics in the Murray–Darling Basin, Federation Press, 2007.
de Beurs, K. M. and Henebry, G. M.: Spatio-temporal statistical methods for modeling land surface phenology, edited by: Hudson, I. L. and Keatley, M. R., Springer, Dordrecht, 2008.

BGD
11, 7685–7719, 2014

de Jong, R., Verbesselt, J., Schaepman, M. E., and Bruin, S.: Trend changes in global greening and browning: contribution of short-term trends to longer-term change, Glob. Change Biol., 18, 642–655, doi:10.1111/j.1365-2486.2011.02578.x, 2012.

Donohue, R. J., McVicar, T. R., and Roderick, M. L.: Climate-related trends in Australian vegetation cover as inferred from satellite observations, 1981–2006, Glob. Change Biol., 15, 1025–1039, doi:10.1111/j.1365-2486.2008.01746.x, 2009.

Dougherty, R. L., Edelman, A., and Hyman, J. M.: Nonnegativity-, monotonicity-, or convexity-preserving cubic and quintic hermite interpolation, Math. Comput., 52, 471–794, 1989.

Ganguly, S., Friedl, M. A., Tan, B., Zhang, X., and Verma, M.: Land surface phenology from MODIS: characterization of the Collection 5 global land cover dynamics product, Remote Sens. Environ., 114, 1805–1816, doi:10.1016/j.rse.2010.04.005, 2010.

Goddard Space Flight Center: Tropical Rainfall Measuring Mission Project TRMM_3B43.v7 product, USGS/Earth Resources Observation and Science (EROS) Center, Sioux Falls, South Dakota, available at: http://trmm.gsfc.nasa.gov/, 2014.

Heberger, M.: Australia's Millennium Drought: impacts and responses, in: The World's Water, edited by: Gleick, P. H., Island Press/Center for Resource Economics, 97–125, 2011.

Huete, A., Didan, K., Miura, T., Rodriguez, E. P., Gao, X., and Ferreira, L. G.: Overview of the radiometric and biophysical performance of the MODIS vegetation indices, Remote Sens. Environ., 83, 195–213, 2002.

Huete, A., Miura, T., Yoshioka, H., Ratana, P., and Broich, M.: Indices of vegetation activity, in: Biophysical Applications of Satellite Remote Sensing, edited by: Hanes, J. M., Springer Remote Sensing/Photogrammetry, Springer, Berlin Heidelberg, 1–41, 2014.

Hufkens, K., Friedl, M., Sonnentag, O., Braswell, B. H., Milliman, T., and Richardson, A. D.: Linking near-surface and satellite remote sensing measurements of deciduous broadleaf forest phenology, Remote Sens. Environ., 117, 307–321, doi:10.1016/j.rse.2011.10.006, 2012.

IPCC: Climate Change 2001: Impacts, Adaptation, and Vulnerability, Contribution of Working Group II to the Third Assessment Report of the Intergovernmental Panel on Climate Change (IPCC), Cambridge University Press, Cambridge, 2001.

IPCC: Climate Change 2007: Impacts, Adaptation and Vulnerability, Contribution of Working Group II to the Fourth Assessment Report of the IPCC, Cambridge University Press, Cambridge, 2007.

BGD
11, 7685–7719, 2014

IPCC: Climate Change 2013: The Physical Science Basis, Contribution of Working Group I to the Fifth Assessment Report of the Intergovernmental Panel on Climate Change, Cambridge University Press, Cambridge, 2013.
Keatley, M. R., Chambers, L. E., and Phillips, R.: Australia and New Zealand, in: Phenology: an Integrative Environmental Science, edited by: Schwartz, M. D., Springer, Dordrecht, 2013.
Kingsford, R. T., Brandis, K., Thomas, R. F., Crighton, P., Knowles, E., and Gale, E.: Classifying landform at broad spatial scales: the distribution and conservation of wetlands in New South Wales, Australia, Mar. Freshwater Res., 55, 17–31, 2004.
Kirby, M., Connor, J., Bark, R., Qureshi, E., and Keyworth, S.: The economic impact of water reductions during the Millennium Drought in the Murray–Darling Basin, AARES conference, 7–10, 2012.
Köppen, W.: The thermal zones of the Earth according to the duration of hot, moderate and cold periods and of the impact of heat on the organic world (translated and edited by: Volken, E. and Brönnimann, S.), Meteorol. Z., 1, 351–360, 1884.
Leblanc, M., Tweed, S., Van Dijk, A., and Timbal, B.: A review of historic and future hydrological changes in the Murray–Darling Basin, Global Planet. Change, 80–81, 226–246, doi:10.1016/j.gloplacha.2011.10.012, 2012.
Lehmann, E. L. and D'Abrera, H. J. M.: Nonparametrics: Statistical Methods Based on Ranks, Holden-Day, 1975.
Liang, L. and Schwartz, M.: Landscape phenology: an integrative approach to seasonal vegetation dynamics, Landscape Ecol., 24, 465–472, doi:10.1007/s10980-009-9328-x, 2009.
Loik, M., Breshears, D., Lauenroth, W., and Belnap, J.: A multi-scale perspective of water pulses in dryland ecosystems: climatology and ecohydrology of the western USA, Oecologia, 141, 269–281, doi:10.1007/s00442-004-1570-y, 2004.
Lymburner, L., Tan, P., Mueller, N., Thackway, R., Lewis, A., Thankappan, M., Randall, L., Islam, A., and Senarath, U.: The National Dynamic Land Cover Dataset, Geoscience Australia, Symonston, Australia, 105 pp., 2011.
Ma, X., Huete, A., Yu, Q., Coupe, N. R., Davies, K., Broich, M., Ratana, P., Beringer, J., Hutley, L. B., Cleverly, J., Boulain, N., and Eamus, D.: Spatial patterns and temporal dynamics in savanna vegetation phenology across the North Australian Tropical Transect, Remote Sens. Environ., 139, 97–115, doi:10.1016/j.rse.2013.07.030, 2013.

BGD
11, 7685–7719, 2014

McMahon, T. A., Murphy, R., Little, P., Costelloe, J. F., Peel, M. C., Chiew, F. H. S., Hayes, S., Nathan, R. J. R. J., and Kandel, D. D.: Hydrology of Lake Eyre Basin, Natural Heritage Trust, Canberra, Australian Capital Territory, 2005

Moulin, S., Kergoat, L., Viovy, N., and Dedieu, G.: Global-scale assessment of vegetation phenology using NOAA/AVHRR satellite measurements, J. Climate, 10, 1154–1170, doi:10.1175/1520-0442(1997)010<1154:GSAOVP>2.0.CO;2, 1997.

Myneni, R. B., Keeling, C. D., Tucker, C. J., Asrar, G., and Nemani, R. R.: Increased plant growth in the northern high latitudes from 1981 to 1991, Nature, 386, 698–702, 1997.

NASA Land Processes Distributed Active Archive Center: MOD13A1 and MOD13C2, USGS/Earth Resources Observation and Science (EROS) Center, Sioux Falls, South Dakota, available at: https://lpdaac.usgs.gov/, 2014.

Nemani, R. R., Keeling, C. D., Hashimoto, H., Jolly, W. M., Piper, S. C., Tucker, C. J., Myneni, R. B., and Running, S. W.: Climate-Driven increases in global terrestrial net primary production from 1982 to 1999, Science, 300, 1560–1563, 2003.

Nicholls, N.: The El Niño/Southern Oscillation and Australian vegetation, Vegetatio, 91, 23–36, doi:10.1007/BF00036045, 1991.

Nicholls, N., Drosdowsky, W., and Lavery, B.: Australian rainfall variability and change, Weather, 52, 66–72, doi:10.1002/j.1477-8696.1997.tb06274.x, 1997.

OzFlux: Australian and New Zealand Flux Research and Monitoring, available at: http://www.ozflux.org.au/, 2014.

Peñuelas, J., Rutishauser, T., and Filella, I.: Ecology, phenology feedbacks on climate change, Science, 324, 887–888, doi:10.1126/science.1173004, 2009.

Philippon, N., Martiny, N., Camberlin, P., Hoffman, M. T., and Gond, V.: Timing and patterns of ENSO signal in Africa over the last 30 years: insights from normalized difference vegetation index data, J. Climate, 27, 2509–2532, doi:10.1175/JCLI-D-13-00365.1, 2014.

Pitman, A. J.: The evolution of, and revolution in land surface schemes designed for climate models, Int. J. Climatol., 23, 479–510, doi:10.1002/joc.893, 2003.

Ponce Campos, G. E., Moran, M. S., Huete, A., Zhang, Y., Bresloff, C., Huxman, T. E., Eamus, D., Bosch, D. D., Buda, A. R., Gunter, S. A., Scalley, T. H., Kitchen, S. G., McClaran, M. P., McNab, W. H., Montoya, D. S., Morgan, J. A., Peters, D. P. C., Sadler, E. J., Seyfried, M. S., and Starks, P. J.: Ecosystem resilience despite large-scale altered hydroclimatic conditions, Nature, 494, 349–352, available at:

BGD
11, 7685–7719, 2014

http://www.nature.com/nature/journal/v494/n7437/abs/nature11836.html#supplementary-information, 2013.
Primack, R. B. and Miller-Rushing, A. J.: Broadening the study of phenology and climate change, New Phytol., 191, 307–309, doi:10.1111/j.1469-8137.2011.03773.x, 2011.
Restrepo-Coupe, N., Huete, A., Broich, M., and Davies, K.: Phenology validation, in: AusCover Good Practice Guidelines: a Technical Handbook Supporting Calibration and Validation Activities of Remotely Sensed Data Products, edited by: Soto-Berelov, M., TERN AusCover, 2014.
Richardson, A., Jenkins, J., Braswell, B., Hollinger, D., Ollinger, S., and Smith, M.-L.: Use of digital webcam images to track spring green-up in a deciduous broadleaf forest, Oecologia, 152, 323–334, doi:10.1007/s00442-006-0657-z, 2007.
Richardson, A. D., Keenan, T. F., Migliavacca, M., Ryu, Y., Sonnentag, O., and Toomey, M.: Climate change, phenology, and phenological control of vegetation feedbacks to the climate system, Agr. Forest Meteorol., 169, 156–173, doi:10.1016/j.agrformet.2012.09.012, 2013.
Risbey, J. S., Pook, M. J., McIntosh, P. C., Wheeler, M. C., and Hendon, H. H.: On the remote drivers of rainfall variability in Australia, Mon. Weather Rev., 137, 3233–3253, doi:10.1175/2009MWR2861.1, 2009.
Savitzky, A. and Golay, M. J. E.: Smoothing and differentiation of data by simplified least squares procedures, Anal. Chem., 36, 1627–1639, doi:10.1021/ac60214a047, 1964.
Schwartz, M.: Introduction, in: Tasks for Vegetation Science, edited by: Schwartz, M., Springer, Netherlands, 3–7, 2003.
Schwartz, M. D.: Preface, in: Phenology: an Integrative Environmental Science, edited by: Schwartz, M. D., Springer, Dordrecht, 2013.
Stone, R. C., Hammer, G. L., and Marcussen, T.: Prediction of global rainfall probabilities using phases of the Southern Oscillation Index, Nature, 384, 252–255, 1996.
Tan, B., Morisette, J. T., Wolfe, R. E., Gao, F., Ederer, G. A., Nightingale, J., and Pedelty, J. A.: An enhanced TIMESAT algorithm for estimating vegetation phenology metrics from MODIS data, IEEE J. Sel. Top. Appl., 4, 361–371, doi:10.1109/JSTARS.2010.2075916, 2011.
Trenberth, K. E. and Caron, J. M.: The Southern Oscillation revisited: sea level pressures, surface temperatures, and precipitation, J. Climate, 13, 4358–4365, doi:10.1175/1520-0442(2000)013<4358:TSORSL>2.0.CO;2, 2000.
United Nations: Global Drylands: a UN System-Wide Response, Geneva, Switzerland, 2011.

BGD
11, 7685–7719, 2014

van Dijk, A. I. J. M., Beck, H. E., Crosbie, R. S., de Jeu, R. A. M., Liu, Y. Y., Podger, G. M., Timbal, B., and Viney, N. R.: The Millennium Drought in southeast Australia (2001–2009): natural and human causes and implications for water resources, ecosystems, economy, and society, Water Resour. Res., 49, 1040–1057, doi:10.1002/wrcr.20123, 2013.

Walker, J. J., de Beurs, K. M., Wynne, R. H., and Gao, F.: Evaluation of Landsat and MODIS data fusion products for analysis of dryland forest phenology, Remote Sens. Environ., 117, 381–393, 2012.

Walker, J. J., de Beurs, K. M., and Wynne, R. H.: Dryland vegetation phenology across an elevation gradient in Arizona, USA, investigated with fused MODIS and Landsat data, Remote Sens. Environ., 144, 85–97, doi:10.1016/j.rse.2014.01.007, 2014.

White, M. A., Thornton, P. E., and Running, S. W.: A continental phenology model for monitoring vegetation responses to interannual climatic variability, Global Biogeochem. Cy., 11, 217–234, 1997.

Young, W. J. and Kingsford, R. T.: Flow variability in large unregulated dryland rivers, in: Ecology of Desert Rivers, edited by: Kingsford, R. T., Cambridge University Press, Cambridge, 2006.

Zhang, X., Friedl, M. A., and Schaaf, C. B.: Monitoring vegetation phenology using MODIS, Remote Sens. Environ., 84, 471–475, 2003.

Zhang, X., Friedl, M. A., and Schaaf, C. B.: Sensitivity of vegetation phenology detection to the temporal resolution of satellite data, Int. J. Remote Sens., 30, 2061–2074, 2009.

Zhang, X. Y., Friedl, M. A., and Tan, B.: Long-term detection of global vegetation phenology from satellite instruments, in: Phenology and Climate Change, edited by: Zhang, X., InTech, 2012.

Zhang, Y., Susan Moran, M., Nearing, M. A., Ponce Campos, G. E., Huete, A. R., Buda, A. R., Bosch, D. D., Gunter, S. A., Kitchen, S. G., Henry McNab, W., Morgan, J. A., McClaran, M. P., Montoya, D. S., Peters, D. P. C., and Starks, P. J.: Extreme precipitation patterns and reductions of terrestrial ecosystem production across biomes, J. Geophys. Res.-Biogeo., 118, 148–157, doi:10.1029/2012JG002136, 2013.

BGD
11, 7685–7719, 2014

Table 1. Percentage distribution of most significant correlation relationship between monthly SOI and phenological peak magnitude per land cover class across the MDB. Shown are percentages of the MDB occupied by different land cover, percentage of basin-wide significantly correlated areas per land cover, percent of significantly correlated land cover class and average rho value per land cover.

Aggregated land cover classes (LCC)	Percent of basin covered by each LCC	% of the areas of significant correlations between monthly SOI and peak magnitude within each LCC	% of each LCC where significant correlation between monthly SOI and peak magnitude occurred	Average ρ of significant correlations within LCC
Trees	43.0	48.7	5.2	0.71
Shrubs	9.8	12.2	5.7	0.74
Grasses	19.0	22.7	5.4	0.72
Rain-fed agriculture and pasture	28.1	15.9	2.6	0.69
Irrigated agriculture and pasture	0.1	< 0.0	0.9	0.69

BGD
11, 7685–7719, 2014

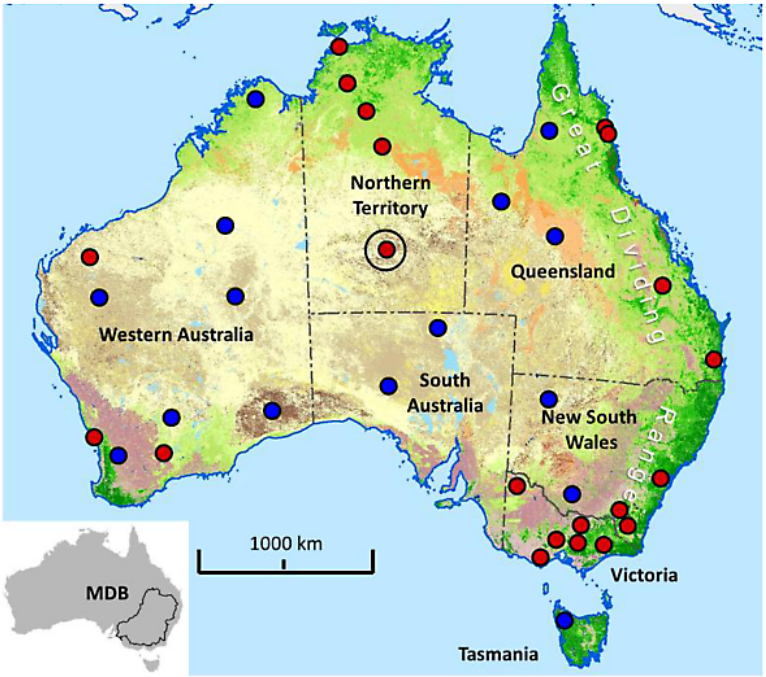

Figure 1. Land cover map of Australia shows closed and open tree cover in dark and light green, respectively. The purple colors that occur predominantly in the south-west and south-east represent crops and pasture. Brown marks shrubs, orange colors mark tussock grass and light brown colors mark hummock grass cover across most of the semi-arid and arid interior (Lymburner et al., 2011). The most prominent topographic feature is the Great Dividing Range that runs along the eastern seaboard. Locations of the 21 OzFlux flux tower sites and 15 additional sites are shown as red and blue circles and were used for phenological trajectory evaluation. The phenology for the site marked by a large black circle is presented and discussed in Sect. 2.2.3. The bottom left panel shows the extent of the MDB.

BGD
11, 7685–7719, 2014

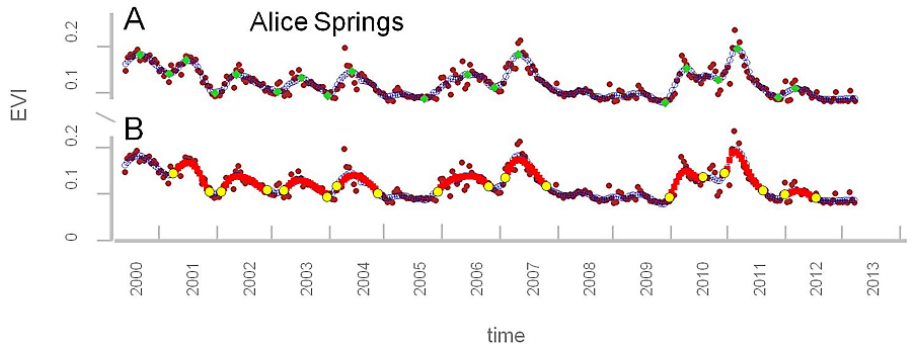

Figure 2. Algorithm steps applied to the 14 year MODIS EVI trajectory (MOD13C2 single 5.6 km pixel) for the Alice Springs flux site representing semi-arid mulga (Acacia) woodland of the center of Australia. **(A)** EVI time series after screening out low quality observations (brown circles), EVI time series after gap filling and smoothing (blue circles), and flagged minimum and peak of cycle points (green diamonds). **(B)** Curves fitted as 7 parameter double logistic functions (red squares) characterizing the phenological cycles, and identifying start and end of cycles points (yellow circles) delineating the cycles. The timing, length, amplitude, and magnitudes of the phenological cycles at the site vary inter-annually.

BGD
11, 7685–7719, 2014

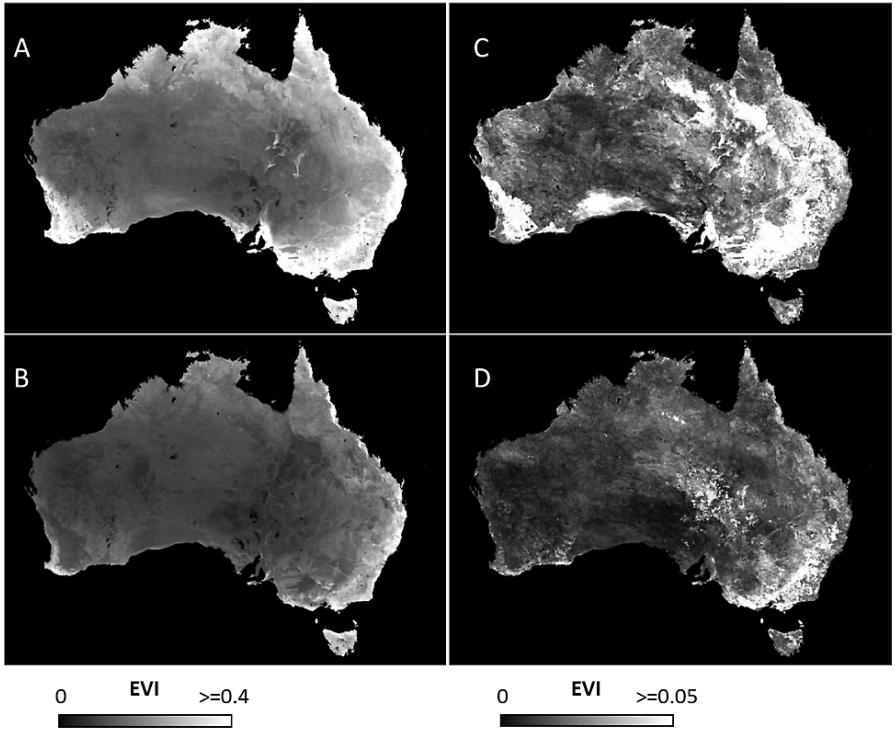

Figure 3. Mean of peak magnitude **(A)**, mean of minimum magnitude **(B)**, standard deviation of peak magnitude **(C)** and standard deviation of minimum magnitude **(D)**. A map of dominant land cover type is provided in Fig. 1.

BGD
11, 7685–7719, 2014

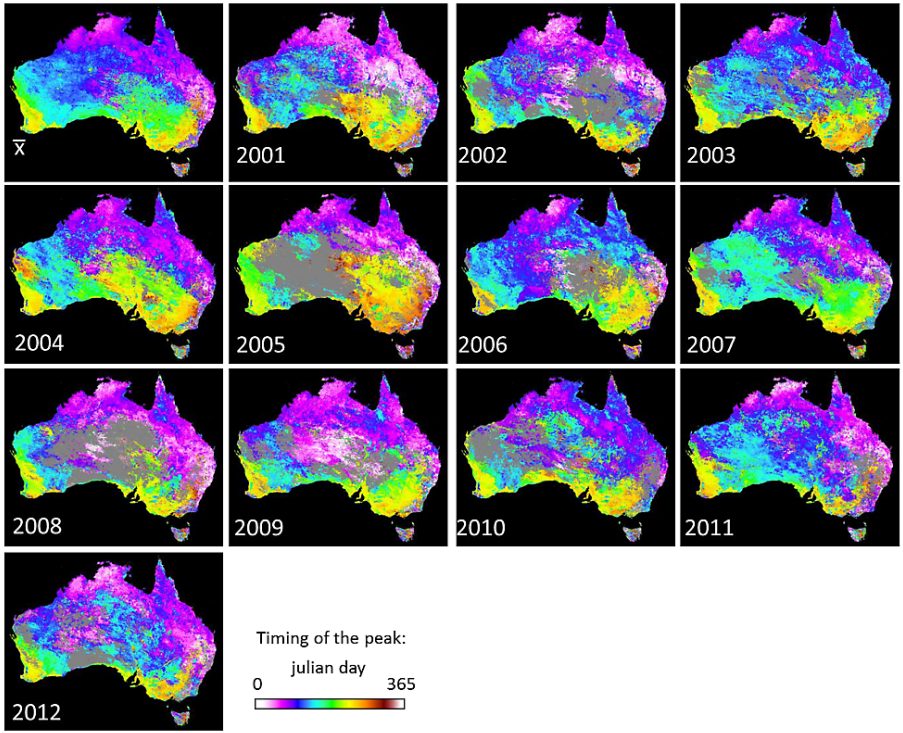

Figure 4. Inter-annual variation in the peak timing. The Julian day of the phenological cycles' peak is displayed in the calendar year when the peak occurred. The mean ($\bar{x}$) of the cycle peak timing is provided for reference. The scale is cyclic. Areas where no peak was observed during a given calendar year are shown in gray.

BGD
11, 7685–7719, 2014

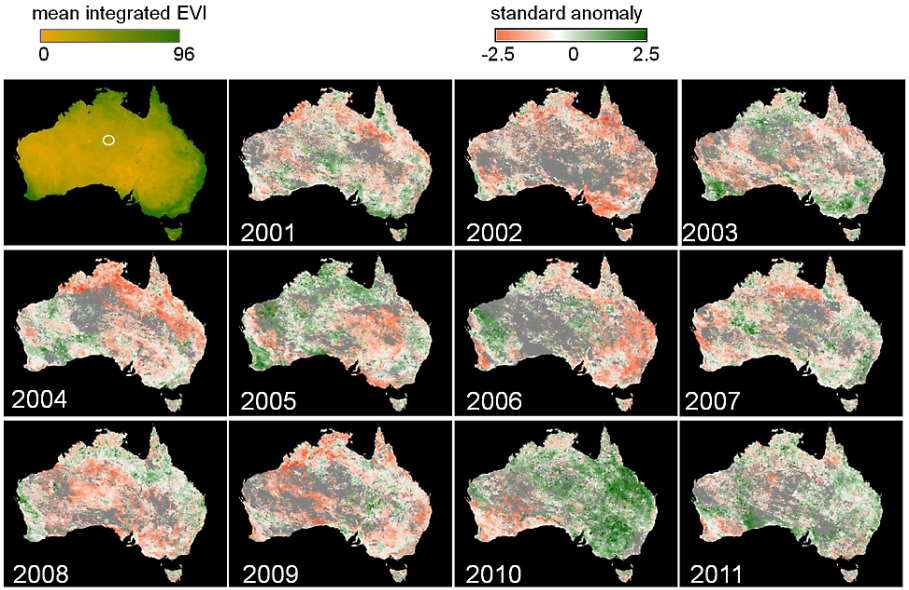

Figure 5. Mean of the cycles' integral greenness across the time series (top left panel in day units) and standardized anomaly of each cycle's integrated greenness. The standardized anomalies of the cycles are shown in the year when the cycle started. For example, for a site with six phenological cycles across the time series that started in 2001, 2002, 2003, 2005, 2008 and 2010, the cycles' standard deviations are shown in 2001, 2002, 2003, 2005, 2008 and 2010. All other years are shown as gray as no phenological cycle start was detected for those years. The white circle in the top left panel mark the OzFlux site shown in Fig. 2.

BGD
11, 7685–7719, 2014

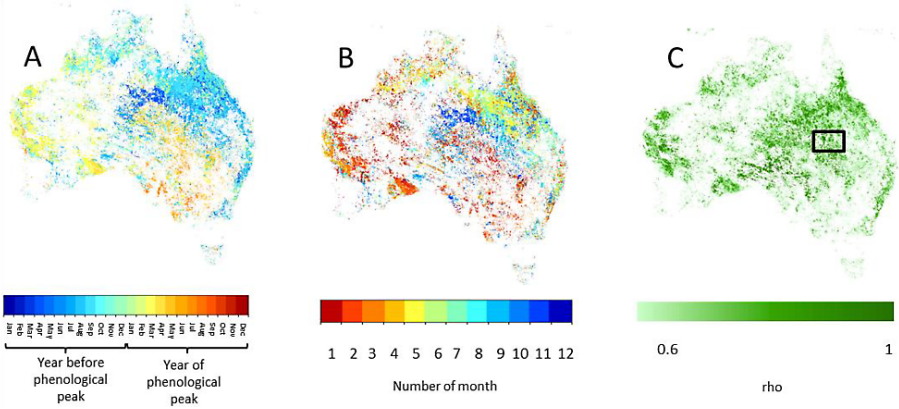

Figure 6. Statistically significant relationships between monthly SOI and phenological cycle peak magnitude. **(A)** SOI month most significantly correlated with peak magnitude. **(B)** Lead time of SOI month relative to phenological peak and **(C)** Spearman's rho. Areas with $p > 0.05$ area shown in white. The black box in the right panel marks the extent of the area shown in Fig. 7 centered on the Cooper Creek floodplain in interior eastern Australia.

BGD
11, 7685–7719, 2014

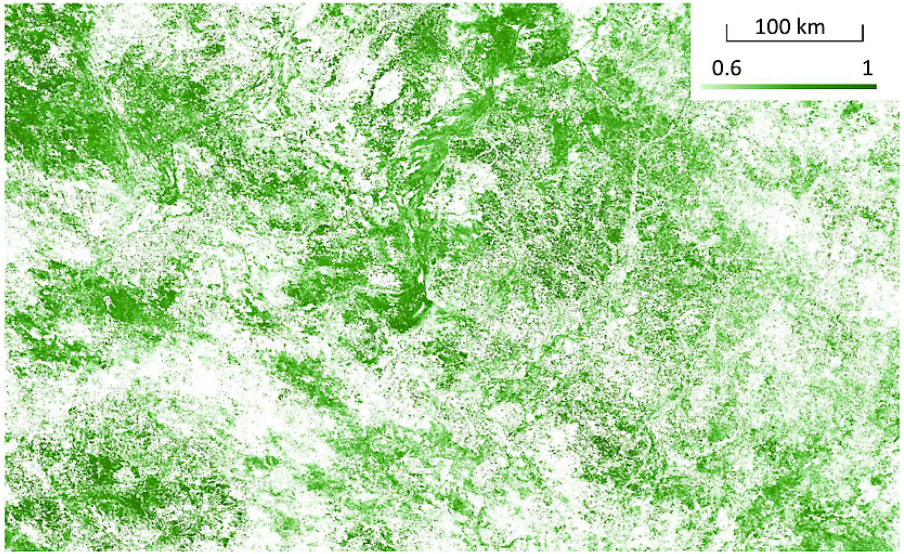

Figure 7. Significant Spearman rho correlations (shown in green) between monthly SOI and phenological cycle peak magnitude over a region in central Australia. The Cooper Creek floodplain is visible in the center. Only areas with $p < 0.05$ and $\rho \geq 0.6$ are shown.

BGD
11, 7685–7719, 2014